Advanced Therapeutics

ADVANCED THERAPEUTICS
www.advtherap.com

RESEARCH ARTICLE OPEN ACCESS

MMP2-Responsive Liposomes Targeting LDLR Enhance the Effectiveness of Anti-Cancer Drugs in Treating Melanoma

Antonio Renda[1] | Antonia I. Antoniou[2] | Marika Quadri[5] | Susanna Comi[1] | Arianna Amenta[2] | Silvia Sesana[1] | Sara Pellegrino[3] | Pierfausto Seneci[2] | Marcus Koch[4] | Vanna Denti[1] | Giuseppe Paglia[1] | Elisabetta Palazzo[5] | Roberta Lotti[5] | Alessandra Marconi[5] | Francesca Re[1,6]

[1]School of Medicine and Surgery, University of Milano-Bicocca, Monza, Italy | [2]Dipartimento di Chimica, Università degli Studi di Milano, Milan, Italy | [3]Department of Pharmaceutical Sciences, University of Milan, Milan, Italy | [4]INM-Leibniz Institute for New Materials, Saarbrücken, Germany | [5]DermoLAB, Department of Surgical, Medical, Dental and Morphological Science, University of Modena and Reggio Emilia, Modena, Italy | [6]Fondazione IRCCS San Gerardo Dei Tintori, Monza, Italy

Correspondence: Alessandra Marconi (alessandra.marconi@unimore.it) | Francesca Re (francesca.re1@unimib.it)

Received: 27 May 2025 | **Revised:** 25 November 2025 | **Accepted:** 8 December 2025

Keywords: drug delivery | liposomes | melanoma | nanoparticles | tumors

ABSTRACT

Current cancer therapies for solid cancers involve surgery, radiotherapy, and chemotherapy, but challenges such as tumor heterogeneity, drug resistance, and poor drug delivery hinder effective treatment. Nano-oncology, specifically liposomes, shows promise by improving drug delivery through better pharmacokinetics and targeting, minimizing toxicity to healthy tissue. Engineered liposomes can enhance drug delivery, and the development of stimuli-responsive nanoparticles offers more precise control over drug release. This study develops a novel all-in-one drug delivery system, using liposomes functionalized with a modified apolipoprotein E peptide (mApoE) for selectively targeting low-density lipoprotein receptor (LDLR) overexpressed on tumor cells and a matrix metalloproteinase 2 (MMP2)-cleavable lipopeptide. The bi-functional liposomes are loaded with Pimasertib, a MAP/ERK kinase inhibitor (MEK1/2), and show enhanced delivery and effectiveness in reducing melanoma cell viability. Furthermore, these liposomes significantly decrease the growth and invasiveness of melanoma 3D spheroids and reduce the expression of epithelial-to-mesenchymal transition markers. These findings highlight the potential of MMP-sensitive, mApoE-functionalized liposomes as effective drug delivery systems for melanoma treatment, providing a promising approach for sustained drug release and targeted therapy in the tumor microenvironment. Moreover, this approach is promising not only for the treatment of melanoma but also for other types of tumors expressing LDLR and MMPs.

1 | Introduction

Current therapeutic approaches for many solid tumors typically involve combinations of surgery, radiotherapy, and chemotherapy, sometimes combined with systemic drug administration. Nevertheless, achieving effective cancer treatment is still difficult due to tumor heterogeneity, drug resistance, and poor drug delivery caused by rapid drug clearance and the presence of biological barriers [1, 2]. Among solid tumors, melanoma, the most aggressive type of skin cancer, shows a poor prognosis mainly attributable to drug resistance, anti-apoptotic mechanisms, tumor metastasis, and immunosuppression. The therapeutic landscape has advanced with the introduction of targeted therapies, such as V-Raf Murine Sarcoma Viral Oncogene

Antonio Renda, Antonia I. Antoniou, and Marika Quadri contributed equally to this work.

Homolog B (BRAF) and MEK inhibitors, and immunotherapies involving checkpoint inhibitors [3, 4]. However, approximately 60% of patients either do not achieve a full response or experience rapid relapse following these treatments [5].

Recently, nano-oncology seems to be a new, promising therapeutic strategy for solid tumors. This therapeutic strategy has improved treatment efficacy through safer and more efficient drug delivery systems that ameliorate pharmacokinetics and drug stability in the bloodstream [2]. Additionally, surface-modified carriers with targeting ligands facilitate precise delivery and help to overcome biological barriers [6].

Among currently available nanoscale drug carriers, liposomes have demonstrated the greatest potential in oncology. These nano-sized, spherical-shaped bilayer phospholipid vesicles enclose an aqueous core and offer numerous advantages, including high drug loading capacity, protection of the drug, improved bioavailability, enhanced intracellular delivery, controlled release, and active targeting of cancer cells. Moreover, significant progress has been made in selectively delivering drugs to tumors. By employing drug-loaded liposomes that utilize both passive and active targeting, toxicity to healthy tissue is minimized, and possible side effects are avoided [7]. Passive targeting primarily leverages the enhanced permeability and retention (EPR) effect found in tumor tissues, which results from inadequate lymphatic drainage and the presence of fenestrated endothelial cells. Active targeting, on the other hand, involves using surface-exposed ligands to identify and bind to antigens expressed by tumor cells, thereby enhancing the delivery of drug carriers [8, 9]. For example, probably to provide cholesterol for sustaining cell proliferation, several tumor cells overexpressed the low-density lipoprotein receptor (LDLR) that can be exploited to design drug delivery systems [10].

To enhance the effectiveness of nano-oncology treatments, the ability to design and develop new, efficient drug delivery systems that control the release of encapsulated drugs is a significant advancement. By modifying the surface of the carriers with various components, these stimuli-responsive nanoparticles (NPs) can react to specific biochemical or physical triggers. This approach ensures greater precision in the timing, dosage, and targeted release of drugs from liposomal carriers. In particular, matrix metalloproteinases (MMPs), a family of zinc-dependent proteases, are involved in the tumorigenesis process of multiple solid tumors. MMPs are implicated in the remodeling of the extracellular matrix through their proteolytic activity, thus allowing tumor progression and metastatization. Still, they also act as cell signaling and immune regulation clues, independent of their catalytic activity [11].

In this study, a novel all-in-one drug delivery system was designed and validated. This approach exploits liposomes functionalized with a modified apolipoprotein E-derived peptide (mApoE), which targets tumor cells by recognizing the overexpressed LDLR. Additionally, a lipopeptide anchored in the liposomal bilayer, cleavable by MMP2, enables controlled drug release in the tumor microenvironment, enhancing specificity and therapeutic efficacy. These bi-functional liposomes were loaded with Pimasertib, a second-generation highly selective inhibitor of the MEK1/2 pathway that is often upregulated in a variety of tumor cells [12]. The results showed that bi-functional liposomes are more effective in delivering Pimasertib to tumor cells. In detail, bi-functionalized liposomes can significantly reduce melanoma cell viability by inducing cell death. Moreover, they significantly decrease the growth area and invasive ability of more complex melanoma 3D spheroids, as well as reduce the expression of Slug and Snail, two epithelial-to-mesenchymal transition (EMT) markers.

2 | Results and Discussion

2.1 | Development of MMP-Responsive Hybrid Lipopeptides

Following the successful, initial approach for the preparation of the MMP-targeted, liposome-compatible constructs, the validated MMP-2 responsive sequence GPLGIAGQ was selected as the better peptide sequence for MMP protease recognition [13]. Subsequently, a fatty acid (stearic acid) and a phospholipid (DOPE) were entailed to play the role of the lipophilic "legs", providing the ability to self-assemble among the natural phospholipids into the liposomal bilayer for the novel hybrid lipopeptides PN-Ac-DOPE, PN-St-DOPE, PS1-St-DOPE, and PS2-St-DOPE, whose structures are shown in Figure 1.

Using MW-SPPS and the standard Fmoc/t-Bu strategy on Wang resin, the responsive sequence GPLGIAGQ was easily synthesized. In order to explore the key condensation between the peptide and a commercial phospholipid in PyBOP-dependent standard amidation conditions (Figure 2), a model acetylated-MMP2-targeted peptide-phospholipid hybrid bearing a direct connection between the phospholipid and the peptide sequence (Figure 2, compound PN-Ac-DOPE, no spacer) was used [14]. This molecule was obtained in excellent yield after reverse-phase HPLC purification and was also used as a control non-responsive molecule during the biological evaluation of lipopeptides, which is referred to below. Then, the acetyl group on the N-terminus was replaced by a lipophilic stearic acid chain, thereby providing hybrid lipopeptide PN-St-DOPE (Figure 2, no spacer), which was prepared using the same protocol in good yield and purity (>98%). Finally, PS1-St-DOPE and PS2-St-DOPE hybrids were also prepared by inserting the appropriate β- (S1, moderate yield) and ε- (S2, good yield) linker between peptide and phospholipid; to investigate the effect of an elongation of the phospholipid from the peptide by adding either a shorter (Figure 2, PS1-St-DOPE, beta-alanine) or a longer spacer (Figure 2, PS1-St-DOPE, 6-aminohexanoic acid).

2.2 | Characterization of Liposomes

Liposomes, embedding MMP-sensitive lipopeptide molecules with a 1:10 mass ratio, were obtained by lipid film hydration followed by probe sonication, and then were surface-functionalized with a mApoE peptide, as previously described [13]. After dilution in PBS pH *7.4*, their size was measured by DLS. All liposomes displayed a <150 nm diameter (Figure 3a) with a 0.2 PDI and a negatively charged surface of about −40 mV (Figure 3b),

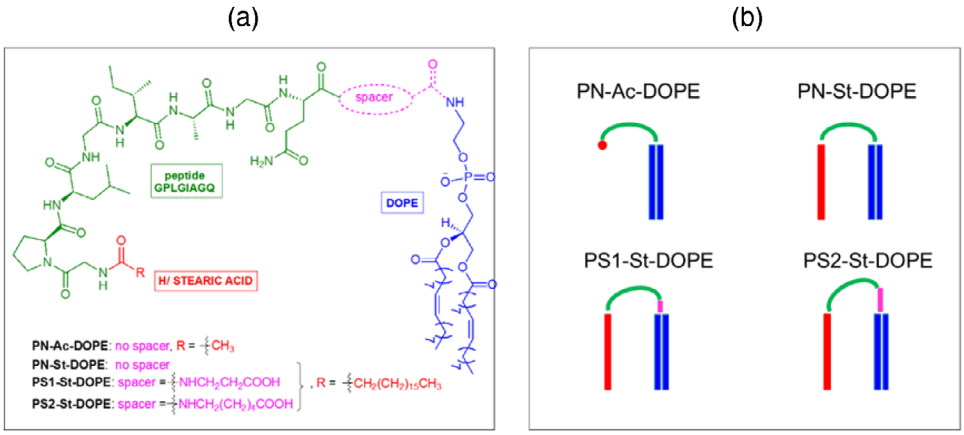

FIGURE 1 | (a) Chemical structures and (b) schematic presentation of hybrid lipopeptides.

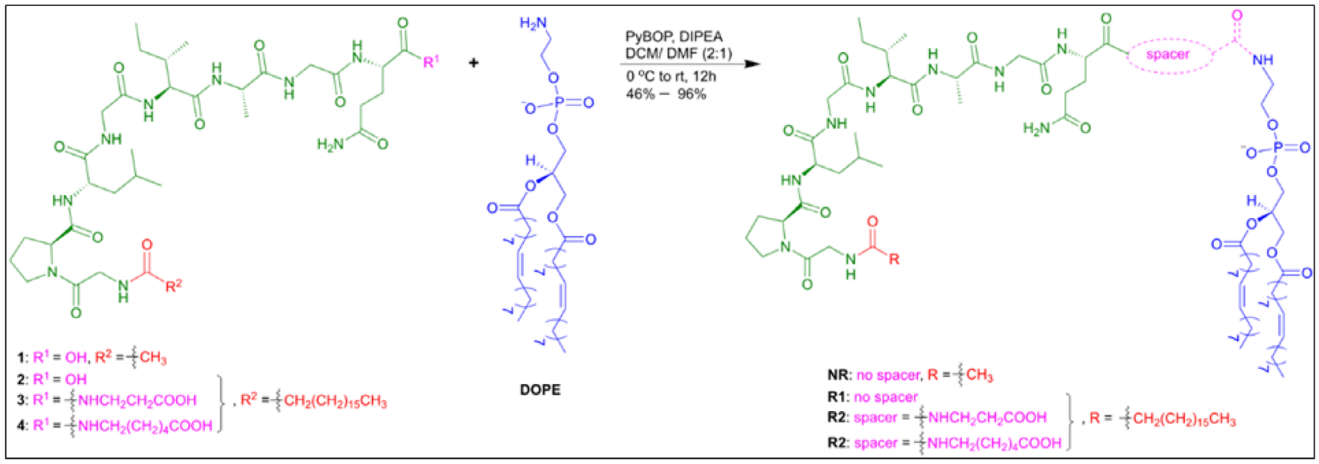

FIGURE 2 | Synthesis of MMP2-sensitive lipopeptide-DOPE hybrids.

slightly higher values than non-functionalized liposomes (110 ± 5 nm diameter, −30 ± 5 mV ζ-potential). These values indicate a monodisperse preparation, not inclined to aggregation. Furthermore, it has been shown that negatively charged liposomes have greater permeability through the skin, so this could also make them promising for topical treatment [15]. The encapsulation efficiency of Pimasertib was 80 ± 10 %, corresponding to a ≈0.2 drug/lipid (D/L) ratio (μmol/μmol). A ≤0.95 D/L ratio denotes a high loading efficacy and the effectiveness of the preparation method, viceversa a D/L ratio >0.95 would indicate a low loading efficiency with high probability of damage to the liposomal membrane [16]. The yield of mApoE coupling on liposomes surface was between 60% and 70%, according to previously published results [17]. Batch-to-batch reproducibility was confirmed by the low variability observed in liposome size, polydispersity index, and encapsulation efficiency across independent preparations, indicating that the dual functionalization process is highly robust and consistent.

Representative cryoTEM images of negatively stained liposomes embedding MMP-sensitive lipopeptide and functionalized with mApoE, before (Figure 3c) and after Pimasertib loading (Figure 3d), are shown, revealing a densely packed dispersion of aggregates consisting mostly of small, spherical, unilamellar vesicles, with diameters ranging between 100 and 200 nm. Slight deviations from the expected spherical shape of the vesicles and the slight aggregation observed on cryoTEM grids might be attributed to the combined effect of staining and drying.

To verify the integrity and stability of liposomes, the fluorescent small molecule probe calcein was entrapped in the liposome core, and its cumulative release was measured at different times. Up to 72 h, MMP-sensitive liposomes showed <0.3 % marginal calcein release, which remained stable until day 7, like non-functionalized liposomes. These results show that liposome batches can retain their contents over time, and their profile is compatible with in vivo use in pharmacological experiments. The better ability of these liposomes to retain their cargo in comparison to data available in literature can be imputable to the presence of Chol that performs a vital role in the stabilization of the liposomal membrane [18]. Additionally, long-term stability of drug-loaded liposomes was determined by measuring the size at + 4 and RT for up to 24 days. The particle size of all liposomal formulations remained stable over 21 days, showing only minor fluctuations between ~140 and 160 nm with no notable differences between storage at 4°C and room temperature (Figure S11). The PDI consistently remained below 0.2 throughout the study.

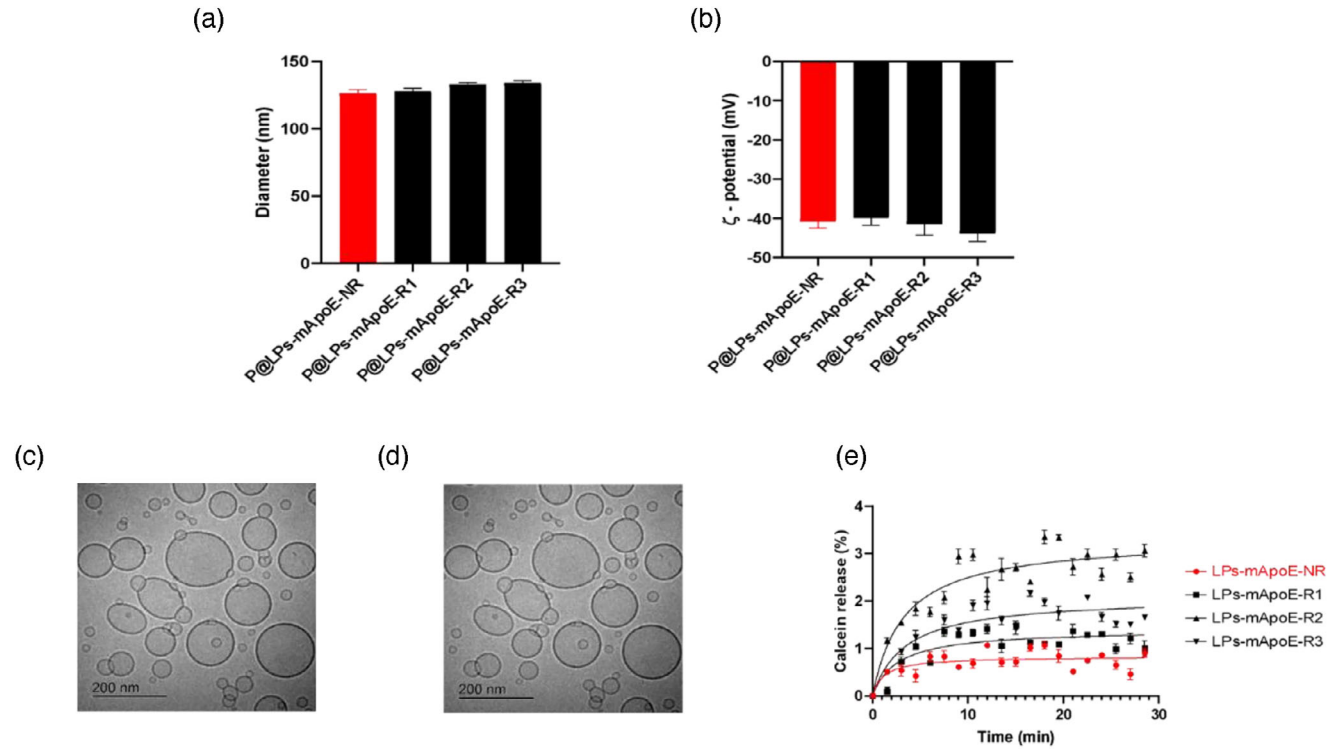

FIGURE 3 | Characterization of liposomes. Liposome embedding MMP-sensitive lipopeptides and functionalized with mApoE were characterized by DLS and Z-pals device, and (a) particle size and (b) surface charge values are shown. (c,d) Representative cryo-EM image of liposomes is shown. The scale bar is embedded in the picture. (e) The responsiveness of liposomes to MMP2 has been determined by measuring the release of embedded calcein from liposomes after incubation with activated MMP2. Data are presented as the mean of three independent experiments ± SD ($n = 32$). Abbreviations: P@LPs, liposomes loaded with Pimasertib, an anticancer drug; –mApoE-NR, liposomes functionalized with mApoE and the non-responsive hybrid lipopeptide; -mApoE-R(#), liposomes functionalized with mApoE and the responsive hybrid lipopeptide.

To evaluate the sensitivity to MMP2, liposomes embedding MMP-sensitive lipopeptides and functionalized with mApoE (LPs-mApoE-R) were loaded with calcein and incubated with 0.2 ng/μL of activated MMP2. Then, the release of the fluorescent probe was measured over time. The results (Figure 3e) showed that the % of calcein release increased about 10 times in the presence of the enzyme, confirming the responsiveness of liposomes to MMP2. Comparing the three different liposomal formulations, the best performing were R2-liposomes, probably due to a better exposure of the MMP2-targeting sequence (GPLGIAGQ peptide) on liposomal surface. Moreover, the lowest % of calcein release displayed by NR-liposomes confirmed the role of stearic acid in destabilizing the liposome bilayer. Comparing these results with those recently published, the liposomes herein designed show a lower MMP2 responsiveness (−50%), suggesting that it is possible to modulate drug release from liposomes by modifying the MMP-sensitive molecule. This strategy will allow for obtaining a sustained drug release, a key feature in the design of drug-delivery systems for cancer therapy [19, 20]. On the basis of these results, liposomes loaded with Pimasertib and bi-functionalized with mApoE peptide and R2 lipopeptide (P@LPs-mApoE-R2) were used for all the following experiments.

To identify the better tumoral model for liposomes validation, three human cell lines were used: A375, a human melanoma cell line, A549, a cell line derived from a human lung adenocarcinoma; and GLI36R, a model of glioma cells. Such cell lines were characterized in terms of MMP2 and LDLR protein levels by Western blot analysis. Cell lines displayed a differential expression profile of both MMP2 and LDLR (Figure S12a,b). A375 cells displayed higher MMP2 and LDLR levels in comparison to A549 and GLI36R. Cells were then treated with P@LPs-mApoE-R2 liposomes for 72 h, and cell viability was assessed by MTT assay. P@LPs-mApoE liposomes, lacking the lipopeptide R2 were used as a control. The results showed that the presence of the lipopeptide-R2 in liposomes confers them the ability to respond to MMP2 present in tumor microenvironments, releasing the embedded Pimasertib that reduced cancer cell viability (Figure S12c–e). The responsiveness of liposomes correlates negatively with MMP2 levels ($r = -0.96$) (Figure S12f). Interestingly, liposomes without lipopeptide were also able to affect the cells' viability of GLI36R and A375, but not of A549, likely due to the low levels of LDLR in these cell lines (Figure S12g).

Mechanistically, the targeting function of mApoE is mediated through its high-affinity interaction with the low-density lipoprotein receptor (LDLR), which is overexpressed in several tumor types, including melanoma. The synthetic mApoE peptide retains the receptor-binding domain of native apolipoprotein E, allowing it to engage LDLR with high specificity. Previous studies have shown that mApoE binding to LDLR is competitive with endogenous ApoE, suggesting that mApoE can effectively mimic the physiological ligand while serving as a targeting moiety for therapeutic delivery [21]. In the context of melanoma, where LDLR upregulation is linked to enhanced lipid metabolism and tumor progression [22], this selective interaction provides a

rational basis for exploiting the mApoE–LDLR axis for targeted drug delivery.

Given the strong response of A375 cells to the P@LPs-mApoE-R2 liposomes, subsequent experiments were conducted on melanoma.

2.3 | Liposomes Decrease Melanoma Cells' Viability and Increase Apoptosis

Given the high heterogeneity of melanoma cells, liposomes were validated on two melanoma cell lines. In particular, WM793B cell lines were derived from a primary vertical growth phase (VGP) tumor, and SKMEL-28, derived from lymph node metastasis (ATCC). The experimental design is reported in Figure 4a. The expression of MMP2 and LDLR protein and their levels were determined by Western blot analysis (Figure 4b). LDLR was expressed by melanoma cell lines, which indicated that liposomes could be effectively recruited by these cells (Figure 4b). On the other hand, only WM793B cells express a high level of pro-MMP2 (inactive), while both cell lines express the active forms (Figure 4b). These differences in MMP2 expression could be associated with their different tumoral progression stages, which correlate to a diverse expression pattern of MMP [23]. This result confirms that melanoma could be potentially be a good target for P@LPs-mApoE-R2 liposomes.

In order to evaluate the effectiveness of liposomes in improving the intracellular delivery of Pimasertib in tumor cells, melanoma cell lines were differently treated in 2D cultures (Figure 4a), as follows: free-drug liposomes (LPs-mApoE-NR); Pimasertib alone (free Pimasertib); liposomes embedding Pimasertib and surface functionalized with mApoE peptide (P@LPs-mApoE) and liposomes embedding Pimasertib and surface functionalized with mApoE peptide and MMP2-sensitive lipopeptide (P@LPs-mApoE-R2). First, different doses of Pimasertib (0.05, 1, and 1.5 μM) were used to assess the most effective ones (Figure S13a). The 0.05 μM dose was the most effective and was then used for subsequent experiments. MTT assay and Flow Cytometry were performed to evaluate cell viability and apoptosis from 24 to 72 h after treatment (Figure 4c,d). The results showed that MM2-sensitive liposomes were the most effective in delivering Pimasertib into tumor cells. In fact, the P@LPs-mApoE-R2 significantly decrease cell viability by increasing the subG1 phase (apoptosis)as compared to the other treatments (Figure 4c,d).

Pimasertib is a highly selective small molecule inhibitor of Mitogen Activated Protein Kinases 1 and 2 (MEK1/2) in the MAPK pathway [24]. To evaluate an effective drug release and intracellular delivery, treated cells were lysed, and the expression of ERK1/2 and p-ERK1/2 was determined by Western blot. A significant reduction in the activation of ERK1/2 in both melanoma cell lines was detected (Figure 4e; Figure S13b). Moreover, a significant reduction of Cyclin B1 and Survivin, a marker of cell proliferation and cell survival, was observed, with a significantly higher reduction in P@LPs-mApoE-R2 liposome-treated cells (Figure 4e; Figure S13b) [25].

All together, these results suggest that the P@LPs-mApoE-R2 liposomes effectively increase drug delivery to melanoma cells.

2.4 | Liposomes Decrease Spheroids Viability and Growth by Increasing Apoptosis

Given the promising results obtained in 2D cell cultures, the study progressed to the development of 3D] culture models by generating cellular spheroids. This approach was chosen as it more accurately mimics the in vivo tumor architecture [26]. The experimental design is shown in Figure 5a. Due to the complex, 3D structure of spheroids, it was decided to increase the liposome dosages compared to 2D experiments. This adjustment was made because treatments might have greater difficulty penetrating the innermost layers, and excessively low doses could have been ineffective. The results showed that 1 μM dose was the most effective, and thus it was used for subsequent experiments (Figure S14a).

Spheroids' viability was evaluated by MTT assay at 24, 48, and 72 h after treatment (Figure 5b). Moreover, spheroids pictures were taken at each time point to calculate spheroid area, which indicate spheroids growth (Figure 5c). The results showed that P@LPs-mApoE-R2 significantly reduced spheroids viability and spheroids area with respect to controls (Figure 5a–c). To understand whether the decrease in the spheroid area depends on cell death, a Propidium Iodide (PI) assay was performed on the spheroids at 24 and 48 h after treatments. A statistically significant increase in cell death in spheroids treated with bi-functionalized liposome as compared to free Pimasertib was observed (Figure 5d).

Taken together, these results confirm the ability of liposomes to improve the bioavailability and the intracellular delivery of Pimasertib to melanoma cells. Given the highly complex and 3D architecture of the spheroid, the findings demonstrate that liposomes are capable of penetrating the spheroid mass, likely guided by LDLR interactions, and effectively releasing the drug within. Furthermore, bi-functionalized liposomes appear to be more effective, as they induce a significant reduction not only in cell viability, but also in the proliferative and growth capacity of spheroids, compared to free Pimasertib or P@LPs-mApoE-NR, indicating that the presence of the MMP-sensitive lipopeptides and the mApoE peptide can increase intracellular delivery of the drug also in a complex 3D structure.

2.5 | Liposomes Decrease the Invasion Ability of Melanoma Spheroids

Melanoma is a highly aggressive skin tumor, given its metastatic potential to spread throughout the body [27]. Moreover, the melanoma microenvironment is known to act as a protective niche that supports tumor growth [28]. Therefore, the aim was to assess the ability of liposomes to enhance the intracellular delivery of the Pimasertib within a context that includes extracellular matrix components, such as collagen, which are integral to the dermis. For this purpose, the analysis was performed exclusively in 3D models, as they appear to be more predictive of the in vivo situation with respect to 2D cultures. Spheroids were then implanted in a collagen I matrix (Figure 6a), which mimics the extracellular microenvironment of the tumor in vivo. After 72 h, spheroids were treated with different modalities, as previously reported. Spheroids images were acquired every 24

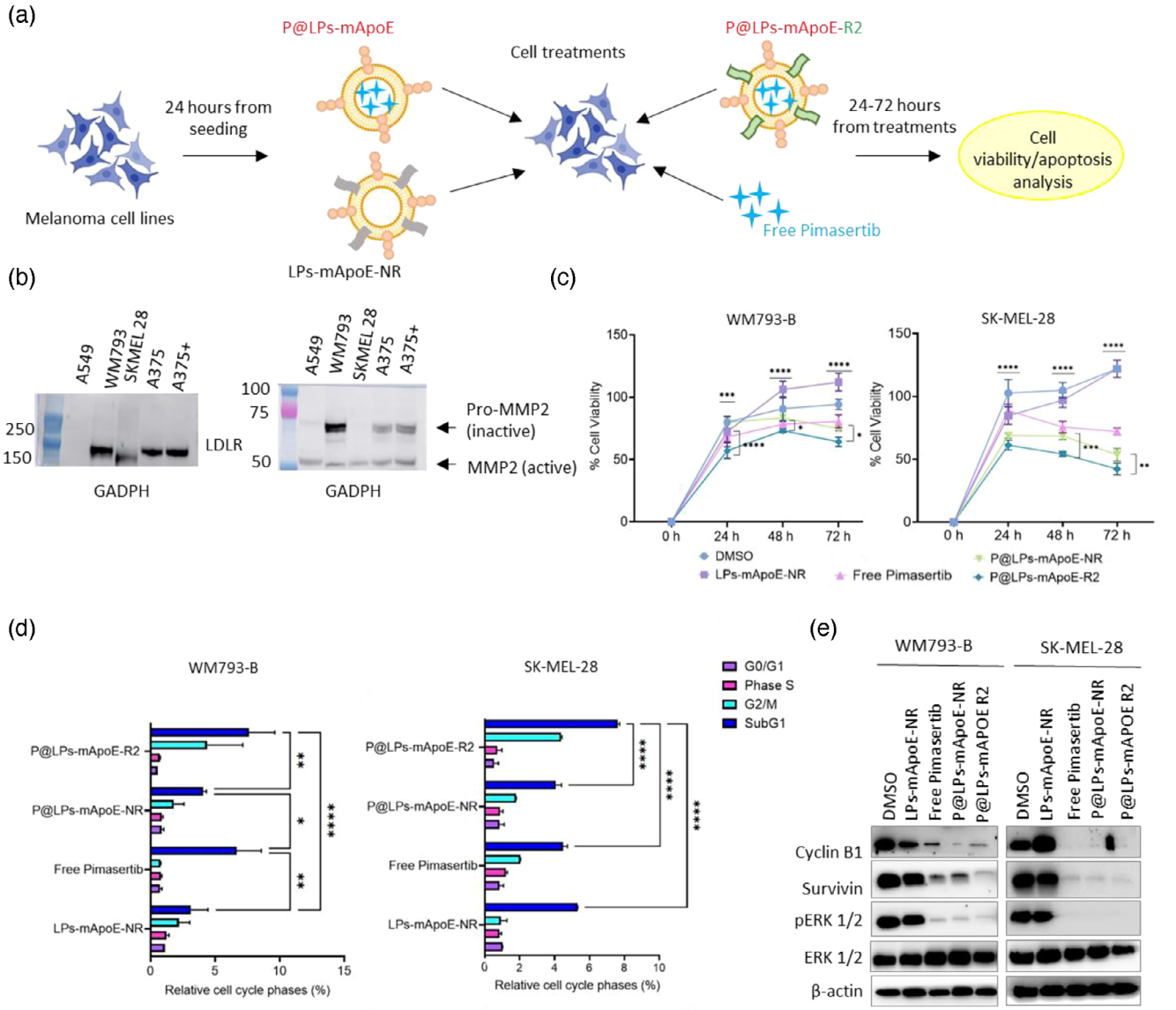

FIGURE 4 | Anti-proliferative effect of liposomes on primary and metastatic melanoma cell lines. (A) Schematic representation of experimental design. Briefly, melanoma cells lines, 24 h from seeding, were treated with DMSO, LPs-mApoE-NR, free Pimasertib, P@LPs-mApoE-NR or P@LPs-mApoE-R2 for 24, 48, and 72 h. Cell viability and apoptosis were evaluated as described in M&M section. This figure was made with BioRender.com. (B) Western blotting shows the levels of MMP2 and LDLR in three different melanoma cell lines; the lung cancer cell line (A549) was used as a negative control. (C) MTT assay and (D) cytofluorimetric analysis (propidium iodide) were performed from 24 to 72 h after treatment. D) Western blotting analysis was performed at 72 h to evaluate the expression level of Cyclin B1, Survivin, ERK1/2, and pERK1/2. βactin was used as control. Statistical analysis was performed using two-way ANOVA. * $0.05 < p < 0.01$, **$0.01 < p < 0.001$, ****$p < 0.0001$. Abbreviations: LPs-mApoE-NR, control liposomes; P@LPs-mApoE-NR, liposomes loaded with Pimasertib and functionalized with mApoE but non-responsive (NR) to MMP; P@LPs-mApoE-R2, liposomes loaded with Pimasertib, embedding the MMP2-responsive lipopeptide R2, and functionalized with mApoE.

h up to 72 h after treatment. The images obtained were then analyzed using the ImageJ software to measure the invasion area of each spheroid and the distance reached by cells invading from spheroids (Figure 6b–e).

Bi-functionalized liposome significantly reduced both spheroid invasion area (Figure 6b,c) and cell invasion distances, as compared to the other treatments (Figure 6e).

The EMT process consists in cell morphological and functional switch from an epithelial to a mesenchymal phenotype and is involved in the initial metastatic process [29, 30]. To evaluate the results, the expression of Slug and Snail, two markers of EMT was analyzed (Figure 5d) [30]. A statistically significant reduction of both Slug and Snail expression in WM793-B cells was detected. Similarly, a significant reduction in Snail expression levels was found in SKMel-28. This reduction is significantly greater in the treatment with bi-functionalized liposomes (P@LPs-mApoE-R2), compared to other treatments, for both cell lines (Figure 5d; Figure S2b).

These results confirm that bi-functionalized liposomes deliver Pimasertib inside 3D spheroids in a more targeted and efficient manner, reducing its invasiveness compared to controls.

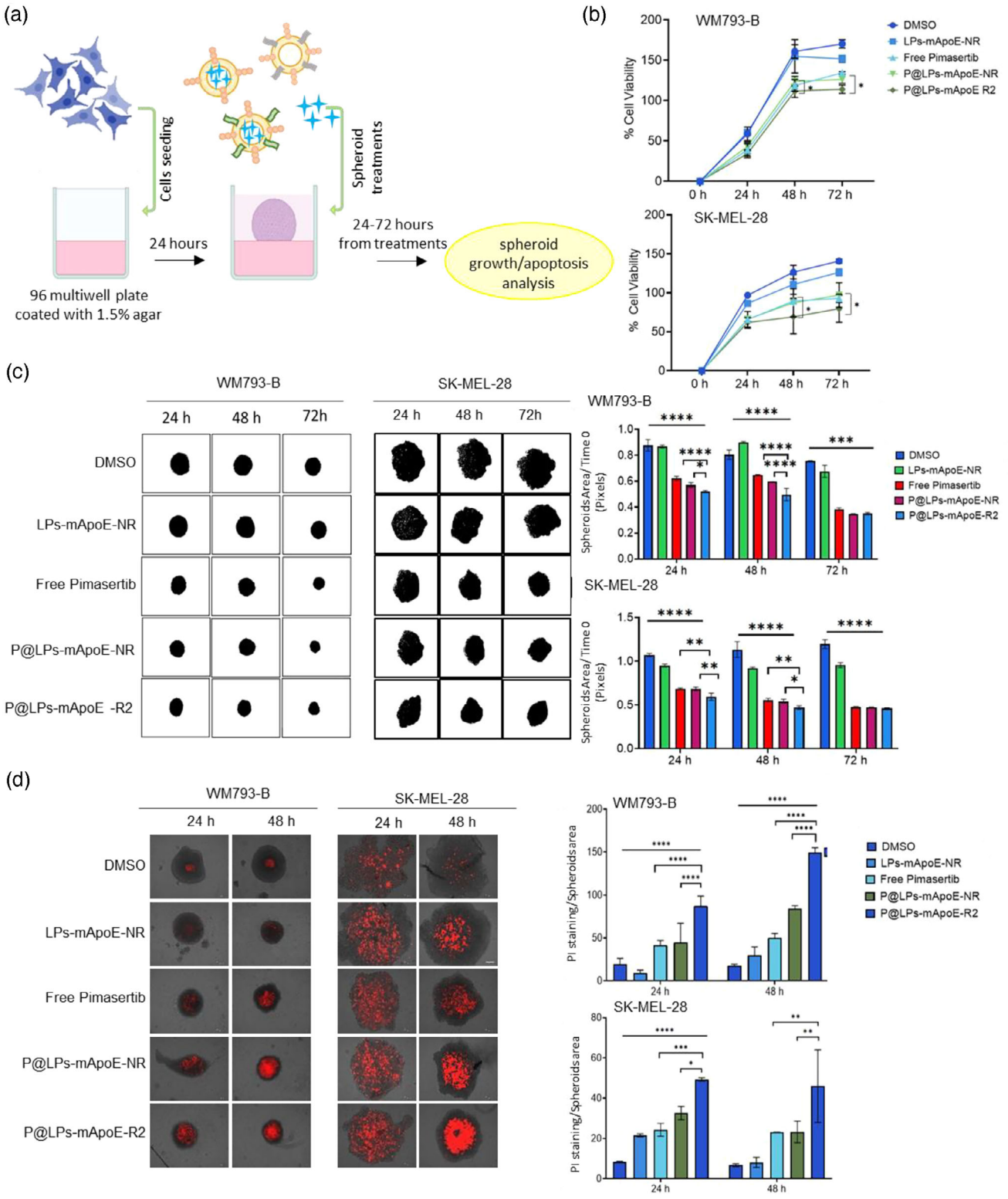

FIGURE 5 | Growth inhibitory effect of liposomes on melanoma spheroids from primary and metastatic cell lines. (A) Schematic representation of experimental design. Briefly, melanoma cells lines were seeded on 1,5% of agar to form 3D spheroids. 24 h from seeding, spheroids were treated with DMSO, LPs-mApoE, free Pimasertib, P@LPs-mApoE-NR or P@LPs-mApoE-R2 drug for 24, 48, and 72 h, and cell viability assay and apoptosis analysis were performed. The figure was made with BioRender.com. (B) MTT assay (C) Spheroids pictures were taken at each time point and analyzed with ImageJ software to calculate spheroids total area. (D) Propidium iodide (PI) assay was performed on melanoma spheroids at 24 and 48 h after treatment. Spheroids' apoptosis was reported as PI staining/spheroids area ratio. Statistical analysis was performed using two-way ANOVA. * $0.05<p<0.01$, ** $0.01<p<0.001$, **** $p < 0.0001$. Abbreviations: LPs-mApoE-NR, control liposomes; P@LPs-mApoE-NR, liposomes loaded with Pimasertib and functionalized with mApoE but non responsive (NR) to MMP; P@LPs-mApoE-R2, liposomes loaded with Pimasertib, embedding the MMP2-responsive lipopeptide R2, and functionalized with mApoE.

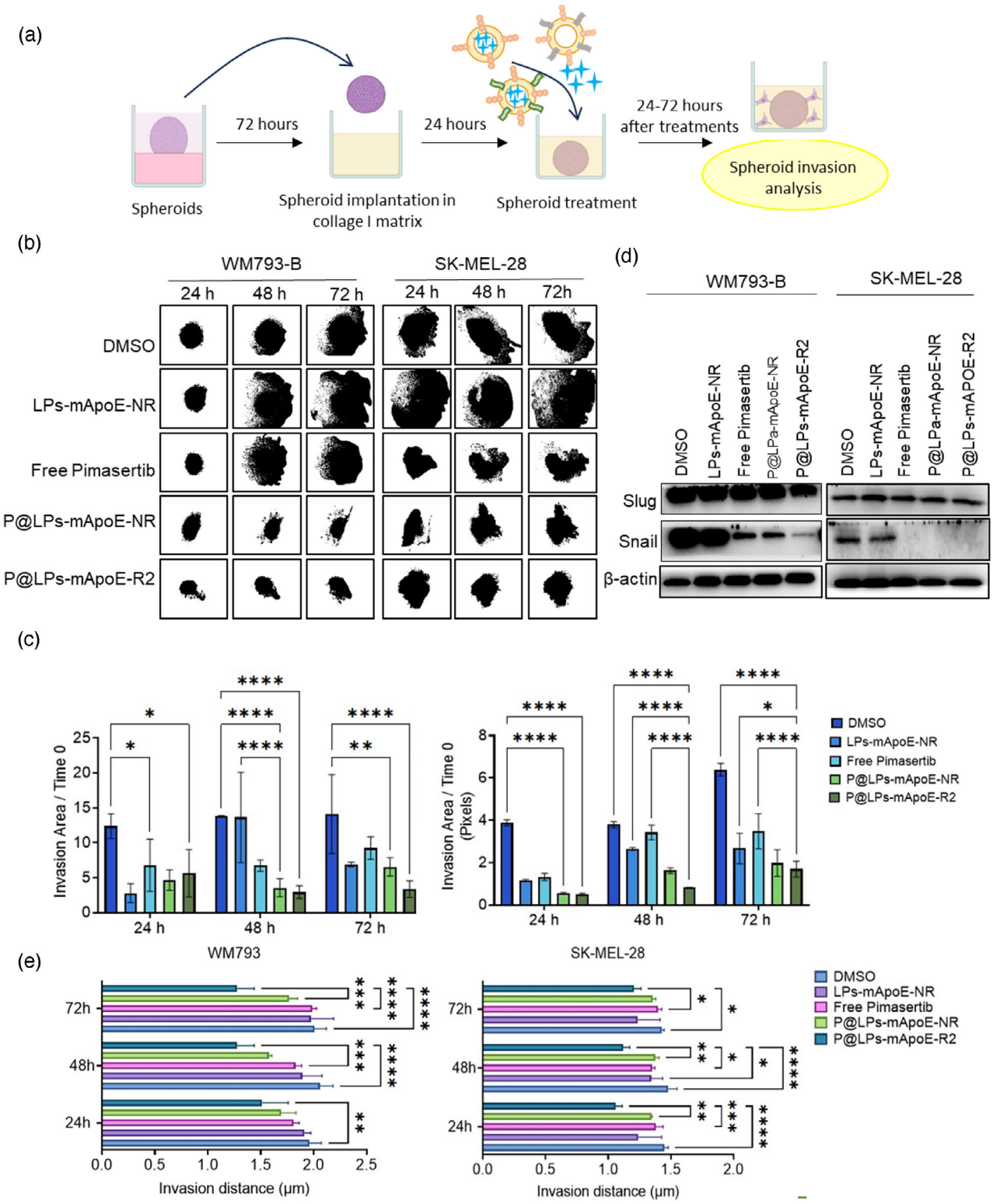

FIGURE 6 | Cell invasion of liposomes in melanoma spheroids from primary and metastatic cell lines. (A) Schematic representation of experimental design. Briefly, melanoma spheroids were incubated for 72 h and then implanted in a matrix of collagen I. After 24 h spheroids were treated as previously reported. Spheroids pictures were taken from 24 to 72 h to evaluate cell invasion from spheroids. The figure was made with BioRender.com (B) Spheroids' pictures were analyzed with ImageJ at each time point, and (C) the invasion area was calculated. (D) Western blot analysis was performed to evaluate the expression levels of EMT markers Slug and Snail. β-actin was used as control. (E) Pictures were analyzed with GIMP software to measure the invasion distance reached by cells from spheroids. Statistical analysis was performed using two-way ANOVA. * $0.05<p<0.01$, ** $0.01<p<0.001$, **** $p<0.0001$. Abbreviations: LPs-mApoE-NR, control liposomes; P@LPs-mApoE-NR, liposomes loaded with Pimasertib and functionalized with mApoE but non responsive (NR) to MMP; P@LPs-mApoE-R2, liposomes loaded with Pimasertib, embedding the MMP2-responsive lipopeptide R2, and functionalized with mApoE.

3 | Conclusion

Melanoma is a highly aggressive and heterogeneous tumor with a low survival rate. Traditional therapy has many shortcomings, including drug side effects and poor patient compliance [31]. For this reason, it is necessary to evaluate new treatment strategies that can overcome the limitations encountered so far.

The aim of this research project was to identify the effectiveness of a new treatment, based on the use of bi-functionalized liposomal nanoparticles, to allow a specific delivery and controlled release of the MEK1/2 inhibitor Pimasertib in in vitro models of melanoma. This approach could overcome the common toxic side effects and bioavailability problems encountered in treatment with the drug in its free form [12, 32]. Based on the results, P@LPs-mApoE-R2 liposomes increase the bioavailability and the intracellular delivery of the drug by reducing parameters such as cell viability, proliferation, and invasiveness in 2D and 3D melanoma models. This innovative targeted drug delivery system has many potential advantages in cancer therapy, promoting a specific, controlled, and more effective intercellular drug delivery in tumor cells. Although further preclinical studies need to be conducted in vivo, these data are particularly encouraging, suggesting that this system, thanks to the mApoE targeting peptide, could potentially increase the bioavailability and the target of any anti-tumoral drug, avoiding undesirable side effects. The targeting function of mApoE relies on its high-affinity, LDLR-specific binding that mimics and competitively interacts with endogenous ApoE, thereby enabling selective delivery to LDLR-overexpressing melanoma cells, potentially reducing lipid uptake and metabolic support to tumor cells.

Interestingly, the presence of the mApoE peptide could also allow the crossing of the blood-brain barrier, which represents one of the preferential sites for melanoma metastasis [13, 33]. Moreover, the lipopeptide anchored in the liposomal bilayer, cleavable by MMP2, enables controlled drug release in the tumor microenvironment, enhancing specificity and therapeutic efficacy.

In conclusion, this new therapeutic approach is promising not only for the treatment of melanoma but also for other types of tumors expressing LDLR and MMPs.

4 | Experimental Section/Methods

4.1 | General Methods—Synthetic Chemistry

All solvents were dried and purified according to standard procedures prior to use. When required, reactions were carried out under a dry nitrogen atmosphere in preflamed glassware. Solvents were routinely removed at ca. 40°C under reduced pressure using a rotary vacuum evaporator. All reagents employed in the present work were commercially available and used without further purification. Flash column chromatography (FCC) was performed on silica gel (70–230 and 230–400 mesh, Merck, Germany) and analytical thin layer chromatography (TLC) on silica gel-F254 precoated glasses (0.25 mm film, Merck, Germany). Spots on the TLC plates were visualized with cerium molybdate stain (Hanessian's stain). The purity of target compounds was determined by reverse phase high performance liquid chromatography (HPLC), with a Jasco LC-NetII/ADC series equipped with a Phenomenex Gemini-NX RP-C18 150 × 4.6 mm, 5 µm particle size column and a MD-4010 PDA detector, and monitoring at 220 nm. Linear gradients of A and B were used, where A = 0.1% TFA in H2O and B = 0.1% TFA in CH3CN, at 0.8 mL/min. Electrospray ionization (ESI)—high resolution mass spectrometry (HRMS) spectra were recorded on a Waters Q-ToF Synapt G2-Si HDMS 8K mass spectrometer, and ESI-MS mass spectra on a Fison MD800 spectrometer.

4.2 | Synthesis of Lipopeptides PN-Ac, PN-St, PS1-St, and PS2-St

Peptide sequences were prepared by microwave (MW)-assisted solid phase peptide synthesis (SPPS) using the Fmoc/t-Bu strategy on Wang resin (100–200 mesh, loading between 0.4 and 0.6 mmol/g) and a Liberty BlueTM automated synthesizer (CEM Corporation, North Carolina). Briefly, every MW synthesis cycle entailed 15 s at 75 oC—170 W followed by 110 s at 90 oC—50 W using a 5 eq. excess of the amino acid (0.2 M in dimethylformamide, DMF), diisopropyl carbodiimide (DIC, 0.5 M in DMF) and ethyl cyano(hydroxyimino)acetate (Oxyma pure, 1 M in DMF) as a coupling system. After final Fmoc-deprotection with 20% piperidine in DMF, the N-terminus was either acetylated with 20 eq. acetic anhydride in the presence of 20 eq. N-methyl morpholine in dichloromethane (DCM, 1 mL/ 100 mg resin) at room temperature for 40 min, or was conjugated with 5.0 eq stearic acid using 4.5 eq. N,N,N,N-tetramethyl-O (1H-benzotriazol-1-yl)uronium hexafluorophosphate (HBTU) as coupling reagent in presence of 6.0 eq N-ethyldiisopropylamine (DIPEA) in DMF at room temperature overnight. Final simultaneous cleavage—side chain deprotection was performed upon treatment of the resin with a solution of 90:2.5:2.5:5 TFA/triisopropylsilane (TIPS)/H2O/phenol at room temperature for 3 h, affording either peptide. Acetyl-GPLGIAGQ-OH (PN-Ac), ESI-MS m/z: [M + Na] + Calcd for C33H55N9NaO11 + 776.39, Found 776.49; or lipopeptides Stearoyl-GPLGIAGQ-OH (PN-St), ESI-MS m/z: [M]- Calcd for C49H87N9O11- 977.65, Found 977.57; Stearoyl-GPLGIAGQβA-OH (PS1-St), ESI-MS m/z: [M + H]+ Calcd for C52H93N10O12 + 1049.70, Found 1049.44, [M + Na] + Calcd for C52H92N10NaO12 + 1071.68, Found 1071.88; and Stearoyl-GPLGIAGQεAhx-OH (PS2-St), ESI-MS m/z: [(M + 2)/2 + H] + Calcd for C55H98N10NaO12+ 569.36, Found 569.36, [M + H + Na]2 + Calcd for C55H99N10NaO122 + 1114.73, Found 1114.00, respectively. Peptide PN-Ac was purified by reverse phase HPLC with an LC-8A chromatograph (Shimadzu Italia, Milan, Italy) equipped with a Phenomenex Gemini-AX RP-C18 250 × 21.2 mm, 5 µm particle size column and a SPD-20A Detector, and monitoring at 220 nm. Linear gradients of A and B were used, where A = 0.1% TFA in H_2O and B = 0.1% TFA in CH3CN. Method: 5–50% B in 40 min: 0–5 min 5% B, 5–45 min 50% B at a flow rate of 20.0 mL/min (Figure S1). Lipopeptides PN-St, PS1-St, and PS2-St were pure enough to be used in the next step without further purification (Figures S2–S4).

4.3 | Synthesis of the Lipopeptide-Phospholipid Hybrids PN-Ac-DOPE, PN-St-DOPE, PS1-St-DOPE, and PS2-St-DOPE

Benzotriazol-1-yloxytripyrrolidinophosphonium hexafluorophosphate (PyBOP, 0.022 mmol, 12 mg) and 1,2-dioleoyl-sn-glycero-3-phosphoethanolamine (DOPE, 0.018 mmol, 13 mg) were added to a vigorously stirred suspension of either peptide PN-Ac or one among lipopeptides PN-St, PS1-St, and PS2-St (0.02 mmol) in 3:1 DCM/DMF (1.2 mL), and the reaction mixture was cooled to 0 oC. Then, N, N-diisopropylethylamine (DIPEA, 0.088 mmol, 15 μL) was added, and the mixture was allowed to gradually warm up to room temperature. After 12 h at room temperature, the mixture was concentrated under reduced pressure and the crude residues toward targets PN-Ac-DOPE, PN-St-DOPE, and PS1-St-DOPE were purified by direct phase FCC (eluent mixture: from 9:1 to 7:3 DCM/MeOH), to provide upon solvent removal compounds PN-Ac-DOPE (28.4 mg, 19.2 μmol, 96%), PN-St-DOPE (22.1 mg, 13.0 μmol, 65%), and PS1-St-DOPE (16.3 mg, 9.18 μmol, 46%) as white solids (Figure 1). As to the purification of PS2-St-DOPE, its poor solubility prevented FCC. Thus, after evaporation of the solvent, the crude was triturated with cold MeOH (2.0 mL) and refrigerated for 2 h. The white precipitate was filtered under vacuo and dried to afford PS2-St-DOPE (26.9 mg, 14.8 μmol, 74%, Figure 1). The hybrid PN-Ac-DOPE was characterized by ESI-MS and HPLC (Figures S5 and S6), whereas hybrids PN-St-DOPE, PS1-St-DOPE, and PS2-St-DOPE were characterized by HRMS (Figures S7–S9).

4.4 | Liposome Synthesis and Characterization

Cholesterol (Chol), sphingomyelin (Sm), and 1,2-distearoyl-sn-glycero3-phosphoethanolamine-N-[maleimide(polyethylene glycol)-2000] (mal-PEG-PE) were purchased from Avanti Polar Lipids Inc., Alabaster, AL, USA. Cleavable lipopeptides were fabricated in-house as described in the previous sections. The modified peptide derived from apolipoprotein E (mApoE, CWG-LRKLRKRLLR) was synthesized by KareBay Biochem, USA.

Unilamellar, nano-sized liposomes were prepared as described [13, 34]. Briefly, liposomes composed of Chol, Sm, mal-PEG-PE, in a 48.75:48.75:2.5 molar ratio were added with lipopeptides, keeping constant the total mass of lipopetides and Sm to 1.0 mg, with a 1:10, lipopeptide:Sm mass ratio. Lipids (dissolved in chloroform) and lipopeptides (dissolved in 8:2 v/v chloroform:methanol) were mixed in a round-bottom flask, and then the solvent was removed through a rotary evaporator. The resulting dried lipid film was hydrated for 1 h by the addition of phosphate-buffered saline (PBS, pH *7.4*) above the lipid phase transition temperature (55°C). After hydration, unilamellar liposomes were obtained by probe sonication in a continuous mode for 20 min with 30% power delivery with a probe-type ultrasound generator (Sonics & Materials, Inc., Newtown, CT, USA) [13]. As to drug loading, Pimasertib (0.5 mg) dissolved in ethanol (0.5 mg/mL) was added to lipids (5 μmol total lipids) dissolved in chloroform (9 mL), and drug-loaded liposomes were prepared as described above. For LDLR targeting, mApoE was added to liposomes in a 1:10 mApoE:mal-PEG-PE molar ratio. Liposomes were purified from non-encapsulated materials by Amicon Ultra 3 kDa Protein Purification and Concentration Filters (Merck, Darmstadt, Germany).

The phosphor content of liposomes was quantified using Stewart's assay, the mApoE binding on liposome surface was detected by measuring their tryptophan fluorescence shift, while Pimasertib loading of liposomes was quantified by LC-MS analysis, using an LC/MS 6546 platform composed by an Agilent 1290 II LC system (Agilent Technologies, Palo Alto, CA, USA) coupled to a TOF-MS spectrometer (Agilent Technologies, Palo Alto, CA, USA) (Figure S10) [17, 35–37].

The hydrodynamic radius, polydispersity index (PDI) and ζ-potential of liposomes were investigated by dynamic light scattering (DLS) with an instrument made by Brookhaven Instruments Corporation, Holtsville, New York, USA equipped with a ZetaPALS device [35, 36].

The morphology of liposomes was characterized by cryo-electron microscopy (cryoEM). Bright-field transmission electron microscopy (TEM) imaging was performed at −170°C and 200 kV accelerating voltage using a JEOL (Tokio, Japan) JEM-2100 LaB6 transmission electron microscope equipped with a Gatan Orius SC1000 CCD camera operating under low-dose conditions, as described [38].

Here below the nomenclature (acronym) of different tested liposomes:

(1) P@LPs-mApoE-R: liposomes embedding Pimasertib and surface-functionalized with both a mApoE peptide and an MMP2-sensitive lipopeptide.

(2) P@LPs-mApoE-NR: liposomes embedding Pimasertib and surface-functionalized with s mApoE peptide and a non-MMP2 responsive lipopeptide.

(3) P@LPs-R: liposomes embedding Pimasertib and surface functionalized with an MMP2-sensitive lipopeptide.

4.5 | In Vitro Cleavage of MMP2-Responsive Liposomes

To assess the in vitro MMP2 responsiveness of liposomes, calcein-loaded liposomes were prepared as described [13]. Liposomes (50 μL) containing 20 μM of lipopetides, were mixed with activated human recombinant MMP2 (50 μL, 0.2 ng/μL R&D Systems) in a black-well plate. Cleavage was performed at 37°C and the fluorescence of released calcein was measured with a GENios Microplate Reader (Tecan Group Ltd., Sitzerland) in kinetic mode for 30 min. Empty and calcein-loaded liposomes without lipopeptides were used as control samples.

4.6 | Cell Cultures

The epithelial cell line A375, originally isolated from the skin of a 54-year-old patient, was used as an in vitro model of malignant melanoma. Cells were maintained in culture in complete DMEM medium supplemented with 10% FBS, 4 mM L-Glutamine, 1%

penicillin-streptomycin (P/S) and 1 mM sodium pyruvate. Cultured cells were maintained at 37°C in a humidified environment and 5% CO2, changing the medium every 2 to 3 days.

The Gli36ΔEGFR-2 cell line (defined in the text and in the figures as GLI36R) was used as an in vitro model of glioblastoma multiforme. Such cells possess a mutation in the EGFR gene called EGFRvIII, present on average in 28–30% of cells isolated from GBM patients [39]. Cells were maintained in culture in complete DMEM medium supplemented with 10% FBS, 4 mM L-glutamine (ECB3000D, Euroclone, Italy), and 1% P/S (ECB3001B, Euroclone, Italy). Cultured cells were maintained at 37°C in a humidified environment and 5% CO2, changing the medium every 2 days [38].

The human alveolar adenocarcinoma cell line A549, originally isolated from a 58-year-old patient, was used as an in vitro model of lung carcinoma. Cells were maintained in culture in complete DMEM/F-12 medium supplemented with 10% FBS, 4 mM L-glutamine, and 1% P/S. Cultured cells were maintained at 37°C in a humidified environment and 5% CO2, changing the medium every other day.

SKMEL28 cells (American Type Culture Collection, Manassas, VA, USA) were maintained in Eagle's Minimum essential medium (EMEM, Lonza, Basel, Switzerland) supplemented with 10% Fetal Bovine Serum (FBS), 2 mM L-glutamine, and 1% penicillin/streptomycin. WM793-B cells (American Type Culture Collection, Manassas, VA, USA) were cultured in Tumor Medium 2% containing: MCDB154CF medium (Thermo Fisher Scientific Inc, Waltham, MA, USA) supplemented with 2% FBS, 1.5 g/L sodium bicarbonate, Leibovitz L-15 medium, 2 mM L-glutammine, 200 mM CaCl2, 5 mg/mL insulin and 1% penicillin/streptomycin (Lonza, Basel, Switzerland).

To obtain 3D multicellular spheroids, the liquid overlay method was used [40]. In detail, 96-well plates were coated with 100 µl of 1.5% agar dissolved in the appropriate melanoma base medium (EMEM or MCB154CF). To sterilize the plate, polymerized agar was irradiated with UVB for 30 min. 5 × 103 melanoma cells per well were seeded and spheroids formation was monitored and photographed after plating. Pictures were analyzed using ImageJ (Wayne Rasband, NIH, USA) software.

4.7 | Measurement of the MMP2 and LDLR Levels of Cell Cultures

The level of MMP2 released from cells was measured by Western Blot (WB) on conditioned media. To obtain the medium conditioned for the growth of different cell lines, cells were cultured either in complete or in serum-free medium for 72 h. Then, the medium was filtered under sterile conditions with a 0.22 µm filter, aliquoted and stored at −80°C until use. On the day of the experiment, the conditioned medium was thawed and the protein content was assessed by the bicinchoninic acid (BCA) microassay. Protein concentration of the samples was calculated using the BSA standard line equation. Samples (30 µg total protein) were loaded onto pre-cast gels (Bolt 4–12% Bis-Tris Plus, Thermo Fisher Scientific). Electrophoretic running was performed in MOPS SDS Running Buffer at a constant 100 V voltage. Subsequently, proteins were transferred onto a nitrocellulose membrane using the iBlot 2 Dry Blotting System (Thermo Fisher Scientific). To verify that the transfer had taken place correctly, the membrane was stained with a Ponceau Red solution. After bleaching, the membrane was incubated with a blocking solution (5% milk in TBS 1X Tween 0.2%) for 1 h at room temperature. Next, the membrane was incubated over-night at + 4°C under gentle agitation with the primary anti-MMP2 antibody (1:250, Thermo Fischer Scientific) diluted in 5% milk, TBS 1X, Tween 0.1%. After the incubation, the membrane was washed with TBS 1X, Tween 0.1% and incubated with the secondary anti-mouse Goat antibody (1:20 000, Invitrogen) conjugated to Horse-Radish Peroxidase (HRP) for 1 h under shaking at room temperature. Finally, membranes were washed with TBS 1X, Tween 0.1% and developed using a solution consisting of Luminol Enhancer and Peroxide Buffer (LiteAblot TURBO, EuroClone) in a 1:1 ratio. Images were acquired using the Amersham Imager 600 instrument (GE Healthcare). A serum-only aliquot under the same conditions was used as a control.

The level of LDLR expressed by cells was measured by WB on total cell protein extract. Briefly, A549, Gli36ΔEGFR-2, and A375 cell lines were plated in Petri dishes (250 000 cells/cm^2) in complete DMEM medium as previously described. At confluence, cells were lysed in RIPA buffer (Thermo Fisher Scientific, Milano, Italy) following the manufacturer's instructions. An aliquot of cell lysate containing 25 µg of total proteins was loaded into gel pre-cast (Bolt 4–12% Bis-Tris Plus, Thermo Fisher Scientific), followed by immunoblotting analysis using anti-LDL Receptor (1:1000, Thermo Fisher Scientific, Milano, Italy). Bands were visualized by an enhanced chemiluminescence system using Amersham Imager 600 (GE Healthcare Srl, Milano, Italy). Data were normalized to β-actin (anti-β-actin 1:5000, Thermo Fisher Scientific, Milano, Italy).

4.8 | MTT Assay

In order to identify the lowest dose at which Pimasertib induced a significant reduction in cell viability, A549, Gli36ΔEGFR-2, and A375 cells were plated in 96-well multiwells (20 000 cells/cm^2) and incubated with increasing doses of free Pimasertib (0.01–1 µM) for 72 h. Then, the metabolic assay based on the conversion of 3-(4,5-dimethylthiazol-2-yl)-2,5-diphenyltetrazolium bromide (MTT) to its insoluble formazan was used to measure cell viability [38, 41]. At the end of the experiment, the optical density at a wavelength of 570 nm was measured using a plate reader (SPECTROstar Nano). Cell viability was calculated in comparison to control (untreated) cells.

To evaluate drug release by MMP-sensitive liposomes and their actual antitumor activity, A549, Gli36ΔEGFR-2 and A375 cell lines were plated in 96-well multiwells (20 000 cells/cm^2) and incubated with MMP-sensitive and MMP-non-responsive liposomes containing Pimasertib. Cells were treated with the drug (1 µM) in complete medium and in complete medium without FBS for 72 h, and their viability was measured by MTT assay.

To evaluate the efficacy of MMP-sensitive liposomes to deliver Pimasertib, WM793B and SKMEL-28 cell line were seeded in 96-well multiwells (5000 cells per well) both in 2D and 3D

condition, as previously reported [40]. After 24 h, cells and spheroids were treated with DMSO, liposomes (P@LPs-mApoE), Pimasertib alone (free drug), liposomes embedding Pimasertib and surface functionalized with mApoE peptide (P@LPs-mApoE drug) and liposomes embedding Pimasertib and surface functionalized with mApoE peptide and MMP2-sensitive lipopeptide (P@LPs-mApoE R2). MTT assay was performed as previously reported [42].

4.9 | Flow Cytometry

SKMEL28 and WM793B cells were treated with DMSO, Free Liposomes (P@LPs-mApoE), Pimasertib alone (Free drug), Liposomes embedding Pimasertib and surface functionalized with mApoE peptide (P@LPs-mApoE drug), and Liposomes embedding Pimasertib and surface functionalized with mApoE peptide and MMP2-sensitive lipopeptide (P@LPs-mApoE R2). After 72 h, cells were trypsinized and resuspended (5 × 105 cells) in 1 mL hypotonic fluorochrome solution containing: 50 μg/mL propidium iodide containing 0.1% sodium citrate, and 0.5% Tryton X-100 (Sigma–Aldrich, Milano, Italy). After 15 min, cells were analyzed using an Epics XL flow cytometer (Coulter Electronics Inc., Hialeah, FL, USA). Apoptosis was detected by evaluating the reduced fluorescence of the DNA-binding dye PI in the apoptotic nuclei.

4.10 | Propidium Iodide Assay

To perform the propidium Iodide assay on 3D melanoma spheroids, melanoma cell lines were seeded in 96-multiwell culture plates previously coated with 1.5% agar in serum-free EMEM or TU2% Medium, supplemented with 0.1% of BSA (Sigma–Aldrich). 24 h after seeding, spheroids were treated with DMSO, Free Liposomes (P@LPs-mApoE), Pimasertib alone (Free drug), Liposomes embedding Pimasertib and surface functionalized with mApoE peptide (P@LPs-mApoE drug) and Liposomes embedding Pimasertib and surface functionalized with mApoE peptide and MMP2-sensitive lipopeptide (P@LPs-mApoE R2). At 24 and 72 h, spheroids were washed twice in PBS (Lonza) and then incubated for 20 min at room temperature with a solution of Propidium Iodide (PI, 10 mg/mL; diluted 1:100 in PBS) (Sigma–Aldrich). Samples were analyzed at a ZOE Fluorescent Cell Imager (Bio-Rad). To quantify PI staining, pictures were analyzed by ImageJ software (NHI). Total spheroids area was measured by ImageJ software and mean values are presented as PI staining/spheroids area.

4.11 | Spheroids Area Analysis

Melanoma cell lines were seeded to generate spheroids. After 24 h of incubation, spheroids were treated with DMSO, free liposomes (P@LPs-mApoE), Pimasertib alone (free drug), liposomes embedding Pimasertib and surface functionalized with mApoE peptide (P@LPs-mApoE drug), and liposomes embedding Pimasertib and surface functionalized with mApoE peptide and MMP2-sensitive lipopeptide (P@LPs-mApoE R2). Pictures were taken from 24 to 72 h and analyzed by using ImageJ software (NIH), as previously described [43]. At least three spheroids were analyzed for each time point. Each photo was analyzed with three different "thresholds" to obtain an average value representing the picture. Total area at each time point was normalized by comparison to its the specific time 0 (day of the treatment). Three biological experiments were performed.

4.12 | Invasion Assay

Melanoma cell lines were seeded to generate 3D spheroids. After 72 h, melanoma spheroids were then implanted in a matrix of type I collagen solution composed as follows: DMEM, 200 nM L-glutamine, 10% FBS, 7.5% sodium bicarbonate, 3 mg/mL type I collagen, previously extracted from rat tails as previously indicated, and 1% penicillin/streptomycin [44]. Collagen solution was distributed in 96-well multiplate (100 μL/well) and allowed to polymerize for 30 min at room temperature. Spheroids were then picked with a 200 μL pipette, implanted in the center of the collagen matrix and, subsequently, overloaded with the appropriate culture medium. The following day, the medium was replaced with medium containing several treatment conditions, as reported above. Spheroids were monitored up to 72 h, pictures were taken from 0 to 72 h and analyzed by using ImageJ software (NIH). Each image was analyzed as previously reported [43]. At least three spheroids were analyzed for each time point. Each photo was analyzed with three different "thresholds" to obtain an average value representing the picture. Invasion area at each time point was normalized by comparison to time 0. Three biological replicates were performed.

4.13 | Statistical Analysis

Statistical analysis on all datasets was performed with GraphPad Prism 8 (GraphPad Software, Boston, US), using the following tests: Two-way ANOVA, one-way ANOVA, unpaired *t* test and Tukey's multiple comparisons test. A <0.05 *p*-value was considered to indicate statistical significance.

Acknowledgements

This research has been supported by Fondazione Regionale per la Ricerca Biomedica: CP2_16/2018 NEVERMIND: New frontiers of engineered nanovectors to improve treatment efficacy and safety in neurological disorders.

Funding

This research was funded by Fondazione Regionale per la Ricerca Biomedica, research project "New frontiers of engineered nanovectors to improve treatment efficacy and safety in neurological–NEVERMIND Project", project number CP2_16/2018.

Conflicts of Interest

The authors declare no conflicts of interest.

Data Availability Statement

All data generated during this study are included in this published article and its supplementary information files.

References

1. R. Kaur, A. Bhardwaj, and S. Gupta, "Cancer Treatment Therapies: Traditional to Modern Approaches to Combat Cancers," *Molecular Biology Reports* 50 (2023): 9663–9676.

2. A. Passaro, M. Al Bakir, E. G. Hamilton, et al., "Cancer Biomarkers: Emerging Trends and Clinical Implications for Personalized Treatment," *Cell* 187 (2024): 1617–1635.

3. A. Boutros, E. Croce, M. Ferrari, et al., "The Treatment of Advanced Melanoma: Current Approaches and New Challenges," *Critical Reviews in Oncology/Hematology* 196 (2024): 104276.

4. R. Lauters, A. D. Brown, and K.-C. A. Harrington, "Melanoma: Diagnosis and Treatment," *American Family Physician* 110 (2024): 367–377.

5. N. Natarelli, S. J. Aleman, I. M. Mark, et al., "A Review of Current and Pipeline Drugs for Treatment of Melanoma," *Pharmaceuticals* 17 (2024): 214.

6. R. Cassano, M. Cuconato, G. Calviello, S. Serini, and S. Trombino, "Recent Advances in Nanotechnology for the Treatment of Melanoma," *Molecules* 26 (2021): 785, https://doi.org/10.3390/molecules26040785.

7. F. Danhier, O. Feron, and V. Préat, "To Exploit the Tumor Microenvironment: Passive and Active Tumor Targeting of Nanocarriers for Anti-cancer Drug Delivery," *Journal of Controlled Release* 148 (2010): 135–146.

8. M. Olsman, V. Sereti, K. Andreassen, et al., "Ultrasound-mediated Delivery Enhances Therapeutic Efficacy of MMP Sensitive Liposomes," *Journal of Controlled Release* 325 (2020): 121–134.

9. M. P. Nikolova, E. M. Kumar, and M. S. Chavali *Pharmaceutics* 14 (2022): 2195, https://doi.org/10.3390/pharmaceutics14102195.

10. G. I. Harisa and F. K. Alanazi, "Low Density Lipoprotein Bionanoparticles: from Cholesterol Transport to Delivery of Anti-cancer Drugs," *Saudi Pharmaceutical Journal* 22 (2014): 504–515.

11. M. J. Kwon, "Matrix Metalloproteinases as Therapeutic Targets in Breast Cancer," *Frontiers in oncology* 12 (2022): 1108695.

12. J.-P. Delord, A. Italiano, A. Awada, et al., "Selective Oral MEK1/2 Inhibitor Pimasertib: a Phase I Trial in Patients with Advanced Solid Tumors," *Targeted Oncology* 16 (2021): 37–46.

13. S. Giofrè, A. Renda, S. Sesana, et al., "Dual Functionalized Liposomes for Selective Delivery of Poorly Soluble Drugs to Inflamed Brain Regions, " *Pharmaceutics* 14 (2022): 2402.

14. K. Peqini, S. Attanasio, L. Feni, G. Cappelletti, and S. Pellegrino, "Breaking down and Building up Alpha-Synuclein: an Insight on Its N-Terminal Domain," *Journal of Peptide Science* 30 (2024): 3556.

15. G. Bozzuto and A. Molinari, "Liposomes as Nanomedical Devices," *International journal of nanomedicine* 10 (2015): 975–999.

16. M. Chountoulesi, N. Naziris, N. Pippa, and C. Demetzos, "The Significance of Drug-to-lipid Ratio to the Development of Optimized Liposomal Formulation," *Journal of Liposome Research* 28 (2018): 249–258.

17. E. Conti, M. Gregori, I. Radice, et al., "Multifunctional Liposomes Interact with Abeta in human Biological Fluids: Therapeutic Implications for Alzheimer's Disease," *Neurochemistry International* 108 (2017): 60–65.

18. P. Nakhaei, R. Margiana, D. O. Bokov, et al., "RETRACTED: Liposomes: Structure, Biomedical Applications, and Stability Parameters with Emphasis on Cholesterol," *Frontiers in Bioengineering and Biotechnology* 9 (2021): 705886.

19. X. Bai, Z. L. Smith, Y. Wang, S. Butterworth, and A. Tirella, *Micromachines* 13 (2022): 1623, https://doi.org/10.3390/mi13101623.

20. V. P. Torchilin, "Multifunctional, Stimuli-sensitive Nanoparticulate Systems for Drug Delivery," *Nature Reviews Drug Discovery* 13 (2014): 813–827.

21. L. Bana, S. Minniti, E. Salvati, et al., "Liposomes bi-functionalized with Phosphatidic Acid and an ApoE-derived Peptide Affect Aβ Aggregation Features and Cross the Blood–brain-barrier: Implications for Therapy of Alzheimer Disease," *Nanomedicine* 10 (2014): 1583–1590.

22. L. Pellerin, L. Carrié, C. Dufau, et al., "Lipid Metabolic Reprogramming: Role in Melanoma Progression and Therapeutic Perspectives," *Cancers* 12 (2020): 3147, https://doi.org/10.3390/cancers12113147.

23. A. Frank, V. David, T.-R. Aurelie, G. Florent, H. William, and B. Philippe, "Regulation of MMPs during Melanoma Progression: from Genetic to Epigenetic," *Anti-cancer agents in medicinal chemistry* 12 (2012): 773–782.

24. O. Von Richter, G. Massimini, H. Scheible, I. Udvaros, and A. Johne, "Pimasertib, a Selective Oral MEK1/2 Inhibitor: Absolute Bioavailability, Mass Balance, Elimination Route, and Metabolite Profile in Cancer Patients," *British Journal of Clinical Pharmacology* 82 (2016): 1498–1508.

25. I. Schütt-Abraham, H. J. Wormuth, and J. Fessel, "Vergleichende untersuchungen zur Tierchutzgerechten elektrobetaubung Verschi edener schlachtgeflugelarten, " *Berliner Und Munchener Tierarztliche Wochenschrift* 100 (1987): 332–340.

26. A. Marconi, M. Quadri, A. Saltari, and C. Pincelli, "Progress in Melanoma Modelling in Vitro," *Experimental Dermatology* 27 (2018): 578–586.

27. B. Ahmed, M. I. Qadir, and S. Ghafoor, "Malignant Melanoma: Skin Cancer-Diagnosis, Prevention, and Treatment," *Critical Reviews in Eukaryotic Gene Expression* 30 (2020): 291–297.

28. B. Arneth, "Tumor Microenvironment", *Medicina* (2019): 56, https://doi.org/10.3390/medicina56010015.

29. S. Lamouille, J. Xu, and R. Derynck, "Molecular Mechanisms of Epithelial–mesenchymal Transition," *Nature Reviews Molecular Cell Biology* 15 (2014): 178–196.

30. X. Ye and R. A. Weinberg, "Epithelial–Mesenchymal Plasticity: a Central Regulator of Cancer Progression," *Trends in Cell Biology* 25 (2015): 675–686.

31. R. W. Jenkins and D. E. Fisher, "Treatment of Advanced Melanoma in 2020 and Beyond," *Journal of Investigative Dermatology* 141 (2021): 23–31.

32. C. Lebbé, A. Italiano, N. Houédé, et al., "Selective Oral Mek1/2 Inhibitor Pimasertib in Metastatic Melanoma: Antitumor Activity in a Phase I, Dose-Escalation Trial, " *Targeted Oncology* 16 (2021): 47–57.

33. F. Pederzoli, G. Tosi, and F. Genovese, "Qualitative and Semi-quantitative Analysis of the Protein Coronas Associated to Different Functionalized Nanoparticles," Affiliations Expand PMID: 29345202, https://doi.org/10.2217/nnm-2017-0250.

34. S. Sesana, F. Re, A. Bulbarelli, D. Salerno, E. Cazzaniga, and M. Masserini, "Membrane Features and Activity of GPI-Anchored Enzymes: Alkaline Phosphatase Reconstituted in Model Membranes," *Biochemistry* 47 (2008): 5433–5440.

35. F. Re, I. Cambianica, S. Sesana, et al., "Functionalization with ApoE-derived Peptides Enhances the Interaction with Brain Capillary Endothelial Cells of Nanoliposomes Binding Amyloid-beta Peptide," *Journal of Biotechnology* 156 (2011): 341–346.

36. B. Ruozi, D. Belletti, A. Tombesi, et al., "AFM, ESEM, TEM, and CLSM in Liposomal Characterization: A Comparative Study," *Int J Nanomedicine* 6 (2011): 557–563, https://doi.org/10.2147/IJN.S14615.

37. J. C. M. Stewart, "Colorimetric Determination of Phospholipids with Ammonium Ferrothiocyanate," *Analytical Biochemistry* 104 (1980): 10–14.

38. L. Taiarol, C. Bigogno, S. Sesana, et al., "Givinostat-Liposomes: Anti-Tumor Effect on 2D and 3D Glioblastoma Models and Pharmacokinetics," *Cancers* 14 (2022): 2978, https://doi.org/10.3390/cancers14122978.

39. R. Nishikawa, X. D. Ji, R. C. Harmon, et al., "A Mutant Epidermal Growth Factor Receptor Common in human Glioma Confers Enhanced Tumorigenicity," *Proceedings of the National Academy of Sciences* 91 (1994): 7727–7731.

40. J. Carlsson and J. M. Yuhas, *Spheroids in Cancer Research* (Springer, 1984).

41. A. Orlando, F. Re, S. Sesana, et al., "Effect of Nanoparticles Binding B-Amyloid Peptide on Nitric Oxide Production by Cultured Endothelial Cells and Macrophages," *International Journal of Nanomedicine* 8 (2013): 1335–1347.

42. M. Quadri, A. Comitato, E. Palazzo, et al., "Activation of cGMP-Dependent Protein Kinase Restricts Melanoma Growth and Invasion by Interfering with the EGF/EGFR Pathway," *Journal of Investigative Dermatology* 142 (2022): 201–211.

43. A. Saltari, F. Truzzi, M. Quadri, et al., "CD271 Down-Regulation Promotes Melanoma Progression and Invasion in Three-Dimensional Models and in Zebrafish," *Journal of Investigative Dermatology* 136 (2016): 2049–2058.

44. N. Rajan, J. Habermehl, M.-F. Coté, C. J. Doillon, and D. Mantovani, "Preparation of Ready-to-use, Storable and Reconstituted Type I Collagen from Rat Tail Tendon for Tissue Engineering Applications," *Nature Protocols* 1 (2006): 2753–2758.

Supporting Information

Additional supporting information can be found online in the Supporting Information section.

Supporting File: adtp70103-sup-0001-SuppMat.docx